Nanostructured Pt–Fe/C cathode catalysts for direct methanol fuel cell: The effect of catalyst composition

Wenzhen Li [a,*], Qin Xin [b], Yushan Yan [c]

[a] Department of Chemical Engineering, Michigan Technological University, Houghton, MI 49931, USA
[b] State Key Laboratory of Catalysis, Dalian Institute of Chemical Physics, Chinese Academy of Sciences, Dalian 116023, China
[c] Department of Chemical and Environment Engineering, and College of Engineering, Center for Environmental Research and Technology (CE-CERT), University of California, Riverside, CA 92521, USA

ARTICLE INFO

ABSTRACT

A series of carbon supported Pt–Fe bimetallic nanocatalysts (Pt–Fe/C) with varying Pt:Fe ratio were prepared by a modified ethylene glycol (EG) method, and then heat-treated under H_2–Ar (10 vol%-H_2) atmosphere at 900 °C. The Pt–Fe/C catalysts were characterized by X-ray diffraction (XRD), transmission electron spectroscopy (TEM), energy dispersive analysis by X-rays (EDX) and induced coupled plasma-atomic emission spectroscopy (ICP-AES). XRD analysis shows that Pt–Fe/C catalysts have small crystalline particles and form better Pt–Fe alloy structure with Fe amount increasing. TEM images evidence that small Pt–Fe nanoparticles homogeneously deposited on carbon support and addition of Fe can effectively prevent Pt particles agglomeration. EDX and ICP-AES show that Fe precursor cannot be fully reduced and deposited on carbon support through the adopted EG reduction approach. The electrochemical surface area of Pt–Fe/C catalyst obtained through hydrogen desorption areas in the CV curve increases with Fe atomic percentage increasing from 0 to ca. 50%, and then decreases with more Fe in the Pt–Fe/C catalyst. RDE tests show that the Pt–Fe/C with a Pt:Fe ratio of 1.2:1 and an optimized lattice parameter of around 3.894 Å has the highest mass activity and specific activity to oxygen reduction reaction (ORR). As cathode catalyst, this Pt–Fe/C (Pt:Fe ratio of 1.2:1) exhibits higher direct methanol fuel cell performance at 90 °C than Pt/C and other Pt–Fe/C catalysts, this could be attributed to its smaller particle size and better Pt–Fe alloy structure.

1. Introduction

Fuel cells provide the final step in hydrogen economy in which chemical energy carried by hydrogen fuel is transformed into electrical energy [1]. Hydrogen fueled proton exchange membrane fuel cells (PEMFCs) have particularly attracted enormous attention, due to their unique features of high energy conversion efficiency, low working temperature, and zero emission [2]. However, the production, transport and storage of hydrogen are facing great technical challenges, and are currently under active research [1]. Compared to H_2/O_2 PEMFCs, direct methanol fuel cells (DMFCs) use liquid methanol as fuel, and do not need bulky fuel reformers, therefore, they are considered as promising mobile or portable power sources in the near future [3–8]. One of the big technical challenges in PEMFCs is the sluggish kinetics of oxygen reduction reaction (ORR) at the cathode: even on the most active Pt surface, the over-potential of ORR is over 200 mV

under open-circuit condition [9,10]. This is even worse for the cathode of DMFCs, a short circuit resulted from methanol crossover from anode will lead to an extra potential loss of >100 mV. This means a total loss of about 25% from the theoretical efficiency only at cathode of DMFCs [2,6–8].

Methanol-tolerant catalysts, such as metal phthalocynines, porphyrins, metal oxides, metal carbides and ruthenium-based chalcogenides, were found to have competitive ORR activity, but their life-times still need to be improved [11–15]. The other strategy is to alloy Pt with other transitional metals to improve ORR activity [16–43]. Carbon supported various binary and ternary alloys of Pt, such as Pt–Co/C, Pt–Cr/C, Pt–Ni/C, Pt–Fe/C and Pt–Cr–Co/C have shown better performance as cathode catalyst than Pt/C in phosphoric acid fuel cells (PAFCs) [18–22], PEMFCs [23–38] and more recently in DMFCs [39–43]. The dispersion and compositional homogeneity of the alloy nanoparticles, which are primarily determined by the preparation and treatment methods, are crucial factors to obtain good electrocatalytic activity [16,17]. The common preparation methods of Pt–M/C consist of a formation of carbon supported platinum (Pt/C), and subsequent deposition of a second transitional metal on Pt/C, and a heat-treatment under inert or reducing atmosphere to facilitating formation of Pt–M alloy structure. This heat-treatment at high temperature generally gives rise to undesired metal particle growth by sintering of platinum particles (e.g. >5 nm), and reduces the surface area of Pt–M/C catalyst [17]. Therefore, it is of paramount importance to prepare Pt–M/C catalysts with small particle size, high specific surface area and uniform size distribution to improve their mass activity of ORR.

Colloid synthesis methods have been emerged as an effective approach to highly active Pt–M alloy/C catalysts, and these methods focus on synthesis of metal nanoparticles colloidal solution, and then deposition of the colloids onto a suitable support material, such as carbon black or activated carbon [17]. An elegant colloid method based on high boiling-point organic solvent, such as phenyl ether, was developed to prepare Fe–Pt magnetic nanoparticles with controlled size, shape and structure [44,45]. This method has been extended to prepare carbon supported Pt–M and Pd–M catalysts (e.g. Pt–Ru, Pt–Fe, Pt–Co, Pt–V–Fe, Pd–Fe, etc) with small and uniform nanoparticles [46–51]. In this synthesis, oleic acid, oelylamine and octadecane were normally used as stabilizers, which are difficult to be completely removed even through a thermal-treatment process at 450–550 °C [46,47]. In addition, the thermal-treatment will lead to Pt–M nanoparticles agglomeration and poor distribution on the carbon supports, eventually limit their electrocatalytic mass activity. In comparison, formations of homogeneous precious metal and precious metal alloy nanoparticles in an ethylene glycol (EG) [52,53] have become a simple electrocatalyst preparation method [8,54–65], because EG can be easily washed away by water. Carbon black and carbon nanotubes (CNTs) supported Pt, Pt–Ru, Pt–Pd and PtSn nanoparticles with small sizes (e.g. <3 nm) and narrow particle distributions (e.g. 2–5 nm) were successfully prepared through the EG method, and they showed improved electrocatalytic activity towards methanol oxidation, ethanol oxidation and oxygen reduction reactions in direct alcohol fuel cell tests [8,54–65].

Pt–Fe has been investigated as a methanol resistant cathode catalyst for DMFC [40,41,43]. In our previous work,

nanostructured Pt–Fe/C catalysts were prepared using the modified EG synthesis method and subsequent heat-treatment at moderated temperature of 300 °C. The Pt–Fe/C showed enhanced ORR activity in a DMFC test. However, we found Fe ions could not be fully reduced and deposited onto carbon support through the EG method [40]. In order to better understand the effect of Pt–Fe composition on the ORR activity in DMFCs, in this article, we prepared Pt–Fe/C catalysts with varying Pt:Fe atomic ratio by a modified EG method, and characterized them by XRD, TEM, EDX, ICP-AES, and studied their electrochemical activity towards ORR in both three-electrode-cells and DMFC single cells.

2. Experimental

2.1. Catalyst preparation

The catalyst support was carbon black Vulcan XC-72 (Cabot Corp., BET: 237 m^2/g, denoted as C) treated by 2 M HCl and 5 M HNO_3 following a procedure reported in Ref. [40]. The aim of this process is to purify XC-72 carbon black and to add some surface functional groups, including carboxyl, hydroxyl and carbonyl groups. Pt–Fe/C catalyst was prepared by EG method developed in our lab [8,40]. The preparation process can be described as follows: hexachloroplatinic (IV) acid (H_2PtCl_6) and iron chloride ($FeCl_3$) solution (The Pt metal loading was 20 wt%, and atomic ratio of Pt:Fe is 3:1, 1:1, 1:3, 1:6, respectively) were mixed well and added to carbon–EG solution (5 vol.%, DI water) by dropping, the Pt concentration is about 1.6 mg per ml EG. 1.0 M NaOH (in EG solution) was added to adjust the pH of the solution to about 11. The mixture was heated to 130 °C for 3 h under a flowing argon (99.5 vol.%) protection. After filtration, washing and drying procedures, the as-prepared Pt–Fe/C sample (denoted as Pt–Fe/C–AR) was obtained. In order to facilitate formation of Pt–Fe alloy structure, the Pt–Fe/C–AR catalysts were heat-treated at 900 °C under H_2/Ar (10 vol.%-H_2) for 1 h, and named Pt–Fe/C-a (3:1), Pt–Fe/C-b (1:1), Pt–Fe/C-c (1:3) and Pt–Fe/C-d (1:6), respectively. The temperature ramp rate is 7 °C/min. As comparison, Pt/C900 catalyst was prepared by a similar EG method as described in Ref. [40], and then was heat-treated at 900 °C under H_2/Ar (10 vol.%-H_2) for 1 h as mentioned above.

2.2. Catalyst characterization

All the Pt-based catalysts were characterized by recording their X-ray diffractiometer (XRD) patterns on a Rigaku Rotalflex (RU-200B) X-ray diffractometer using Cu–K$_\alpha$ radiation with a Ni filter. The tube current was 100 mA and tube voltage was 40 kV. The 2θ angular regions between 20° and 85° were explored at a scan rate of 7°/min and the 64°–72° angular was scanned at 1°/min in order to obtain the mean Pt crystalline size precisely using the Scherrer formula. The angular resolution in all the 2θ-scans was 0.02° for all XRD tests. All the Pt-based catalysts before tests were subjected to energy dispersive analysis by X-rays (EDX) by employing JEOL JSM-5600LV scanning electron microscope with operating voltage of 20 kV to determine the compositions of the catalysts. TEM investigations were carried out in a JEOL JEM-2000EX operating at 100 kV to get information of the mean particle size and size distribution of Pt particles of

the catalysts. Induced couple plasma-atomic emission spectroscopy (ICP-AES) was used to determine the Fe concentration of filtration solvent for preparation of Pt–Fe/C-c catalyst.

2.3. Three-electrode-cell test

Electrochemical characterization was conducted in a conventional three-electrode cell setup with a glassy carbon working electrode, a saturated calomel reference electrode (SCE) and a Pt foil counter electrode. A potentiostat (EG&G 273A) was connected to the three-electrode cell for CV and RDE experiments on the Pt–Fe/C catalysts. 5.0 mg Pt–Fe/C was dissolved in 1.0 mL ethanol and 50 μL Nafion (5 wt%) were ultrasonically blended in a glass vessel for half an hour to obtain a homogeneous ink. A 25 μL suspension was spread on the surface of a glassy carbon electrode with a diameter of 4 mm (0.1256 cm^2 area) using a conventional method-micropipette and dried under 80 °C for 10 min to obtain a thin active catalytic layer. The Pt metal loading on GC is 190 μg/cm^2. The reference electrode used in our experiments has been calibrated by standard hydrogen electrode (SHE) and its relative potential was 0.240 V. All the data were reported versus SHE. The cyclic voltammetry was scanned 20 cycles from 0.04 to 1.0 V (vs. SHE) at the scan rate of 50 mV/s under a high purity nitrogen (99.99%) saturated atmosphere. The ORR polarization curve was obtained at 5 mV/s from 1.24 to 0.34 V (vs. SHE), using a rotating speed of 2500 rpm under oxygen (99.99%) bubbling. The working electrolyte is 1.0 M HClO$_4$ for CV and ORR tests and all tests were conducted at room temperature. The calculations on chemical surface area (particle size is based on XRD results), Pt utilization, mass activity and specific activity can be found in Ref. [40].

2.4. Membrane electrode assembly (MEA) fabrication and DMFC test

The electrochemical activity of these Pt-based cathodic catalysts (metal loading 1.0 mgPt/cm^2) in DMFC was examined. The details of the membrane treatment, electrode preparation and MEA fabrication of the DMFCs can be found in Refs. [8] and [40]. The DMFC was assembled by mounting the MEA into single cell with an active cross-sectional area of 4 cm^2. The single cell polarization curves were collected after the operation condition of single cell has been stable for half an hour. The DMFC was operated as the following conditions: 1.0 M CH$_3$OH, 1.0 mL/min, 90 °C, 0.2 MPa oxygen back pressure.
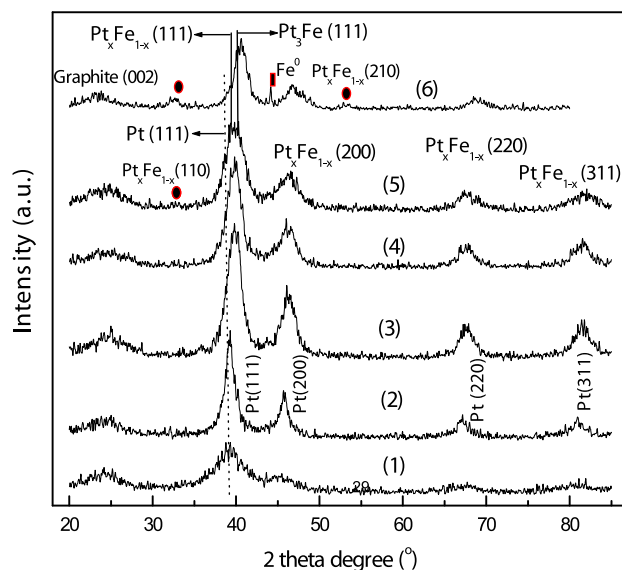

Fig. 1 – Powder XRD patterns of Pt/C and Pt–Fe/C catalysts: (1) Pt/C, (2) Pt/C900, (3) Pt–Fe/C-a, (4) Pt–Fe/C-b, (5) Pt–Fe/C-c, (6) Pt–Fe/C-d.

3. Results and discussion

The atomic ratio of Pt:Fe in the Pt–Fe/C catalyst determined by EDX is 10.5:1 for a, 2.5:1 for b, 1.2:1 for c and 1: 2.9 for d catalyst (as shown in Table 1). The chemical composition of Pt–Fe/C-c catalyst was also determined by bulk analysis gravimetric method, and the atomic ratio of Pt:Fe is 1:1.5. This indicates the ratio of Pt:Fe in the catalyst is larger than the initial ratio of Pt:Fe in the synthesis system for all Pt–Fe/C samples. ICP-AES showed that ca. 70% Fe ion was in the filtration solvent (this can be converted to Pt:Fe ratio of 1.1:1 in the Pt–Fe/C-c). This is because weak reducing agent EG could not fully reduce Fe^{3+} under the adopted experimental conditions, only around 1/2– 1/3 Fe precursors can be reduced and deposited on carbon support. Our recent study on a solution-phase reduction shows strong reducing agent (e.g. LiBet$_3$H) and high reducing temperature (e.g. 285 °C) can fully reduce Fe and Co ions [51].

XRD patterns of these Pt/C and Pt–Fe/C catalysts are shown in Fig. 1. The diffraction peaks at. 39.7°, 46.2°, 67.4° 81.2° observed in diffraction patterns of Pt/C and Pt/C900 catalysts

Sample	Pt:Fe atomic ratio in synthesis system	Pt:Fe atomic ration determined by EDX	Average Pt crystalline size determined by XRD (nm)	Lattice parameter (Å)
Pt/C	–	–	2.4	3.927
Pt/C900	–	–	5.4	3.942
Pt–Fe/C-a	3:1	10.5:1	4.4	3.912
Pt–Fe/C-b	1:1	2.5:1	4.0	3.908
Pt–Fe/C-c	1:3	1.2:1, 1:1.5[a], 1.1:1[b]	3.6	3.894
Pt–Fe/C-d	1:6	1:2.9	3.2	3.856

Table 1 – Compositions, crystalline sizes and lattice parameters of Pt/C and Pt–Fe/C catalysts.

a Determined by gravimetric method.
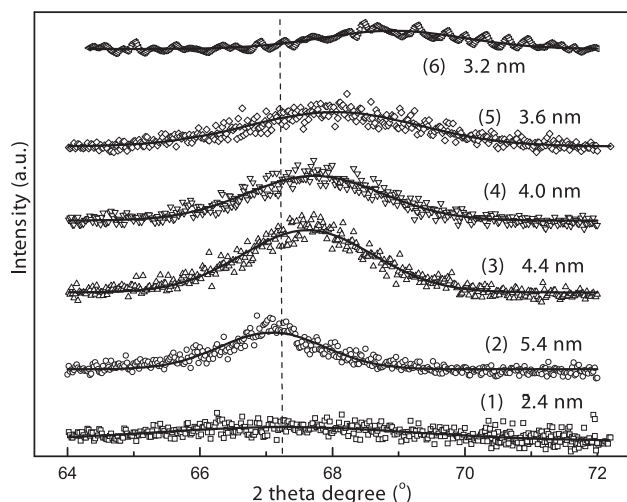b Determined by ICP-AES.

Fig. 2 – Powder XRD patterns of Pt/C and Pt–Fe/C catalysts showing detailed Pt (220) diffraction peak, (1) Pt/C, (2) Pt/C900, (3) Pt–Fe/C-a, (4) Pt–Fe/C-b, (5) Pt–Fe/C-c, (6) Pt–Fe/C-d.

can be attributed to the Pt(111), (200), (220), (311). It is observed that all platinum diffraction peaks in the Pt–Fe/C catalysts were shifted from that of pure Pt to a higher angle of Pt_3Fe alloy. No diffraction peaks of Fe, Fe_2O_3 or other Fe oxides are observed in the XRD patterns of Pt–Fe/C-a, b, c catalysts, which suggests Fe was involved in the formation of Pt–Fe alloy after H_2-reducing treatment at 900 °C. The super-lattice Pt_xFe_{1-x}(110) and (210) are observed in the sample c and d, and Fe^0 diffraction peak is observed at $2\theta = 42.1°$ in the sample-d, which indicate that alloy structure changes with addition of more Fe, and Fe^0 exists when Fe's amount is very high. The average Pt crystalline size of all the Pt/C and Pt–Fe/C catalysts were obtained from Scherrer's formula based on the Pt (220) diffraction peak, and they are shown in Fig. 2 and Table 1. The particle size of Pt/C900, Pt–Fe/C-a, Pt–Fe/C-b, Pt–Fe/C-c and Pt–Fe/C-d is 5.4 nm, 4.4 nm 4.0 nm, 3.6 nm and 3.2 nm,

respectively. Further, it is interesting to note that the lattice parameter for Pt–Fe/C-d decreases to 3.856 Å, which is much smaller than that of Pt–Fe/C-c (3.894 Å). As reported in literature [21,40], the lattice parameter of Pt and Pt_3Fe alloy is 3.924 Å and 3.866 Å respectively, this means that the Pt–Fe/C catalyst can simultaneously have smaller particle size and form better Pt–Fe alloy structure, with Fe contents increasing.

High and homogeneous dispersion of spherical Pt–Fe nanoparticles was obtained for Pt–Fe/C-c catalyst, as can be seen from the TEM image in Fig. 3a. After heat-treatment at 900 °C under H_2/Ar atmosphere, Pt–Fe nanoparticles have narrow size distribution, ranging from 2 nm to 6 nm (as shown in Fig. 3b), which is in sharp contrast with the Pt/C900 sample, which has a wider particle size distribution of 2–12 nm. Some bigger Pt agglomerations were found in Pt/C900 sample (Fig. 3c). These results are in good consistence with the XRD characterizations.

It has been reported that Pt–Ru/C (atomic ratio of 1:1) and Pt–Sn/C have smaller average particle size than Pt/C, when the modified EG method was used to synthesize the Pt–M alloy catalysts [57,59–61]. In the current work, we found addition of Fe can decrease the particle size of Pt–Fe/C as well. According to the XRD results, the average crystalline size of Pt/C is 2.4 nm, while that of the as-prepared Pt–Fe/C-c catalyst is only as small as 1.5 nm (not shown in Fig. 1). After H_2/Ar treatment at 900 °C, Pt/C900 has an average crystalline size of 5.4 nm, which is larger than that of Pt–Fe/C-c (3.6 nm). Very smaller particle size of the as-received Pt–Fe/C-c may be explained as follow: more crystalline nucleus was formed when Fe precursors were added under the adopted synthesis conditions. Therefore, the Pt particle will grow on more nucleus, thus resulting in smaller Pt particle size. Detailed investigation on the synthesis mechanism of the Pt–Fe/C still needs to be carried out in the future.

Fig. 4 shows the CV curves of the Pt–Fe/C catalysts. With Fe amount in the Pt–Fe/C increasing, the hydrogen desorption areas increase and then decrease, which suggests the Pt–Fe/C catalyst has an optimized electrocatalytic active area. The electrochemical surface area of Pt/C, Pt–Fe/C-a, Pt–Fe/C-b, Pt–
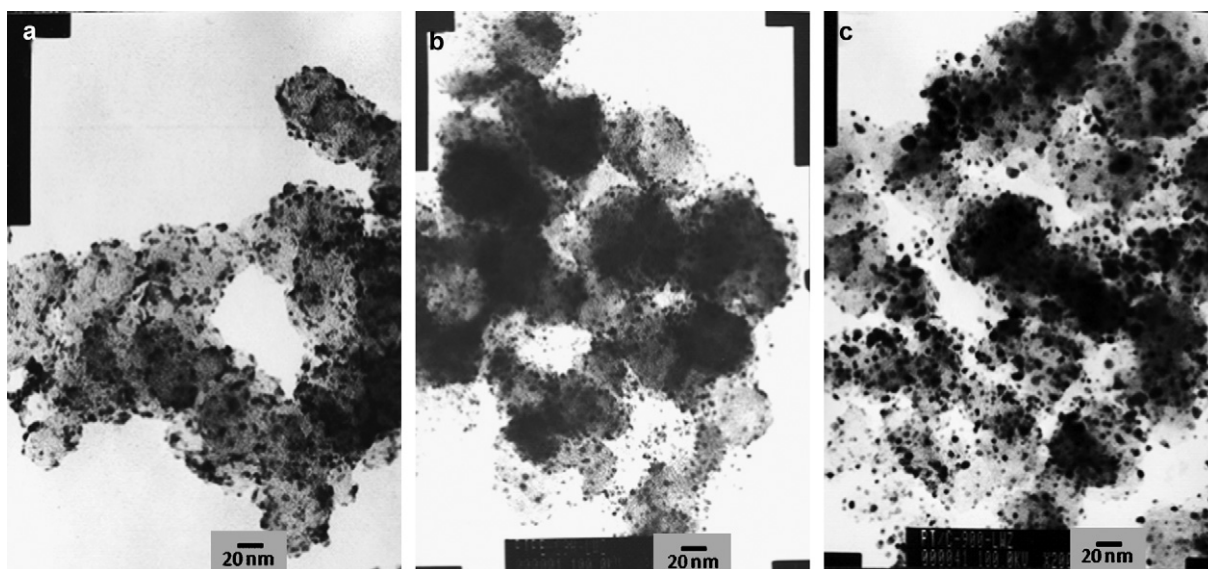

Fig. 3 – TEM images of (a) Pt–Fe/C-c catalyst as-received, (b) Pt–Fe/C-c after H_2/Ar treatment at 900 °C, and (c) Pt/C after H_2/Ar treatment at 900 °C.
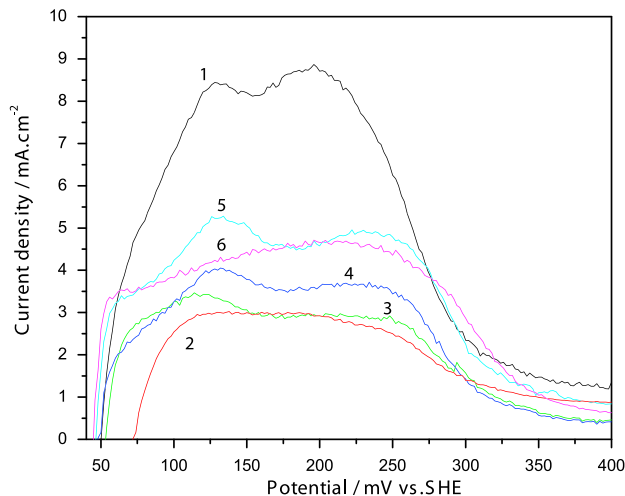
Fig. 4 – Cyclic voltammetry curves of (1) Pt/C, (2) Pt/C900, (3) Pt–Fe/C-a, (4) Pt–Fe/C-b, (5) Pt–Fe/C-c, (6) Pt–Fe/C-d catalysts showing hydrogen desorption peaks on the catalysts, 1.0 M HClO$_4$, 25 °C, 50 mV/s.
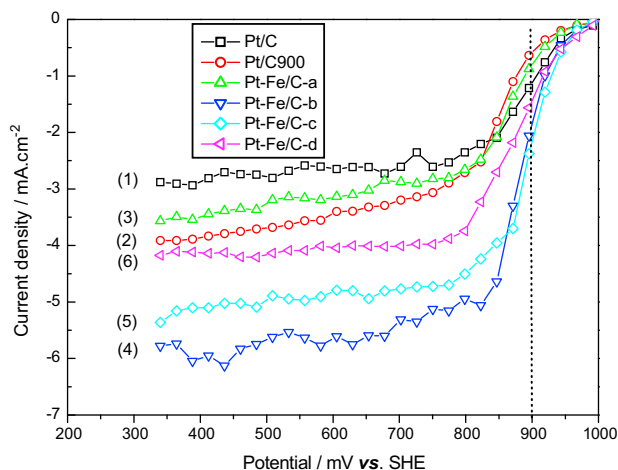

Fig. 5 – Oxygen reduction reaction activity on (1) Pt/C, (2) Pt/C900, (3) Pt–Fe/C-a, (4) Pt–Fe/C-b, (5) Pt–Fe/C-c, (6) Pt–Fe/C-d catalysts in 1.0 M HClO$_4$, 25 °C, 2500 rpm, 5 mV/s, cathodic scan.

Fe/C-c and Pt–Fe/C-d is 68.3, 30.4, 36.6, 46.2 and 41.3 m^2 g^{-1}, respectively. The ECSA of Pt/C900 is only 22.1 m^2 g^{-1}. The Pt utilization of the catalyst is the ratio of its electrochemical surface area to chemical surface area. Pt–Fe/C-c has the highest Pt utilization of 59.3%, which is slightly higher than Pt/C (58.5%). Therefore, high surface area and better Pt–Fe alloy structure can be simultaneously obtained by altering the Fe amount in the Pt–Fe/C catalyst. However, with more Fe amount in the Pt–Fe/C, the Pt utilization decreases. This could be attributed to Fe aggregates on the Pt surface. This result is consistent with previous work reported by Kim et al. [20,21]. Some Fe aggregates were on the surface of large diameter Pt nanoparticles, and reduced the surface area and mass activity of the Pt–Fe/C catalyst.

The ORR activity on the Pt/C and Pt–Fe/C catalysts tested in a three-electrode-cell setup were shown in Fig. 5. With scan potential decreasing, the absolute value of ORR current increases and comes to a plateau around 0.75 V (*vs*. SHE). The currents at 0.9 V (*vs*. SHE) were used to calculate the mass activity and specific activity of the catalysts, which are listed in Table 2. Although Pt/C900 (Pt/C after heat-treatment at 900 °C) has higher specific activity than Pt/C (176 *vs*. 136 mA m^{-2}Pt), it has lower mass activity than Pt/C, because its ECSA reduced to less 1/3 of its original value (from 68.3 to 22.1 m^2 g^{-1}). For Pt–Fe/

C catalysts, with Fe amount increasing, Pt–Fe nanoparticle size becomes smaller and its surface area increases. Further, the lattice parameter shrinks, which means better formation of Pt–Fe alloy structure. Therefore, the mass activity of Pt–Fe/C is higher than Pt/C. Pt–Fe/C-c has the highest mass activity of 19.2 mA mg^{-1}Pt and highest specific activity of 416 mA m^{-2}Pt. Its mass activity and specific activity is 2 times and 3 times higher than Pt/C, respectively. However, with more Fe amount in the Pt–Fe/C catalyst, both mass activity and specific activity goes down. It should be noted that the *absolute* activity reported here is lower than that in the previous work based on 'thin-film' electrode [10], this is because our GC electrode loading is 190 μgPt cm^{-2}, which is higher than 7–30 μgPt cm^{-2} used for 'thin-film' electrode. Since the Pt–Fe/C catalysts will be used in DMFC cathode, which requires higher precious metal loading (e.g. >1.0 mgPt cm^{-2}) than PEMFC cathode (e.g. <0.2 mgPt cm^{-2}). The comparative activities tested in the RDE technique should reflect the right trend of ORR activities on the home-made Pt/C and Pt–Fe/C catalysts.

A 'volcano' type curve of activity as a function of Fe atomic percentage (Fe/(Pt + Fe) in mole, obtained from the Pt–Fe compositions from EDX results) of the Pt–Fe/C catalyst was plotted in Fig. 6a. The optimized Fe atomic percentage is around 50% for both mass activity and specific activity. It is

Sample	Chemical surface area (m^2 g^{-1})	Electrochemical surface area (m^2 g^{-1})	Pt utilization (%)	At 0.9 V (*vs*. SHE)	
				Mass activity (A g^{-1}Pt)	Specific activity (mA m^{-2}Pt)
Pt/C	116.7	68.3	58.5	9.3	136
Pt/C900	51.9	22.1	42.6	3.9	176
Pt–Fe/C-a	63.6	30.4	47.8	5.4	178
Pt–Fe/C-b	70.0	36.6	52.3	14.3	391
Pt–Fe/C-c	77.8	46.2	59.3	19.2	416
Pt–Fe/C-d	87.5	41.3	47.2	12.4	300

Table 2 – Chemical surface areas, Pt utilizations, mass activities and specific activities of Pt/C and Pt–Fe/C catalysts.
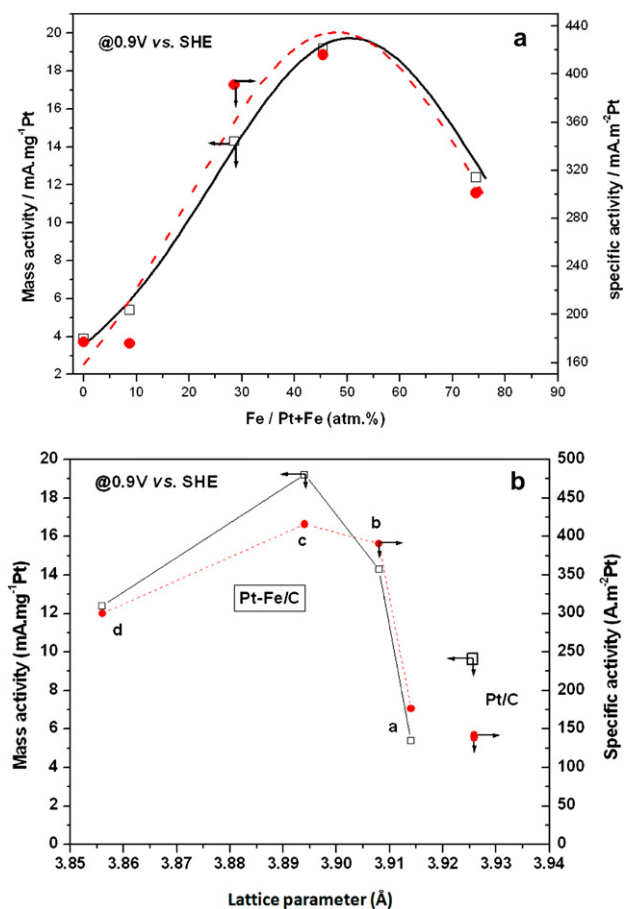
Fig. 6 – Mass activity and specific activity *vs.* Fe atomic percentage in Pt–Fe/C catalyst (a), and *vs.* lattice parameter (b).

found that the ORR activity on the Pt–Fe/C catalyst also shows a 'volcano' type as a function of the lattice parameter of Pt–Fe alloy, as shown in Fig. 6b. The ORR activity improves significantly with lattice parameter decreasing from 3.927 to 3.894 Å, while reduces a little with lattice parameter continuously decreasing from 3.894 to 3.856 Å. The optimized lattice parameter of Pt–Fe alloy is around 3.894 Å.

Since DMFC performance is the ultimate method for evaluating the methanol-tolerant ORR activity on Pt–Fe/C catalysts, we tested the polarization curves of DMFCs (single cell) using the Pt/C and Pt–Fe/C cathode catalysts, as shown in Fig. 7. The DMFC performances of these Pt/C and Pt–Fe/C catalysts based MEAs are in the order: Pt–Fe/C-c > Pt–Fe/C-b > Pt/C > Pt–Fe/C-d > Pt–Fe/C-a > Pt/C900. As observed from Fig. 7, the open-circuit voltage (OCV) of the single cell with Pt–Fe/C-c is 0.687 V, which is close to the one with Pt/C catalyst (0.684 V). This indicates Pt–Fe/C catalyst does not show apparent methanol-tolerant ability. This result is in good agreement with our previous observation based on Pt–Fe/C under moderate temperature (300 °C) treatment [40]. At 0.660 V, the current density of the DMFC with Pt–Fe/C-c and Pt–Fe/C-b is 19.8 mA mg^{-1}$_{Pt}$ and 12.6 mA mg^{-1}$_{Pt}$, respectively, while that of the DMFC with Pt/C is only 3.9 mA mg^{-1}$_{Pt}$. As shown in Fig. 8, the DMFC output potential as a function of Fe atomic percentage demonstrates a similar 'volcano' type at a given operation current density, e.g. at an operation current
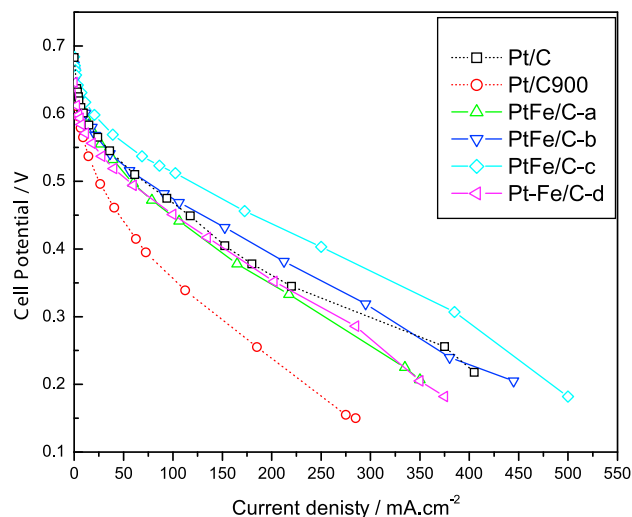

Fig. 7 – Comparison of DMFC polarization curves of the DMFC in presence of Pt/C and Pt/C900 (hollow symbol, dot line); Pt–Fe/C-a, Pt–Fe/C-b, Pt–Fe/C-c and Pt–Fe/C-d (solid symbol, solid line) cathode catalysts (1.0 mgPt/cm^2); anode: Pt–Ru/C (20 wt%Pt, 10 wt%Ru, Johnson Matthey Corp.; catalyst loading: 2.0 mg Pt–Ru/cm^2); electrolyte membrane: Nafion-115$^®$ (Dupont) membranes; operation temperature: 90 °C; Methanol: 1.0 M, 1.0 mL/min, oxygen back pressure: 0.2 M Pa.

density of 40 mA cm^{-2}, the output potential of the DMFC with Pt–Fe/C-c (Pt–Fe ratio of 1.2:1) is 0.552 V, which is higher than any other Pt/C and Pt–Fe/C based DMFCs. These results are in consistence with the RDE results, which strongly support the fact that the DMFC performance enhancement is originated from ORR enhancement of Pt–Fe/C catalyst. Pt–Fe/C-a and Pt/C900 show lower ORR activity and DMFC performance, this is mainly attributed to their poor Pt–Fe alloy structure and small surface areas, resulted from the high temperature (900 °C) treatment. In our study, Pt–Fe/C-c with a Pt–Fe ratio around 1.2:1 has the highest ORR activity in the DMFC test.
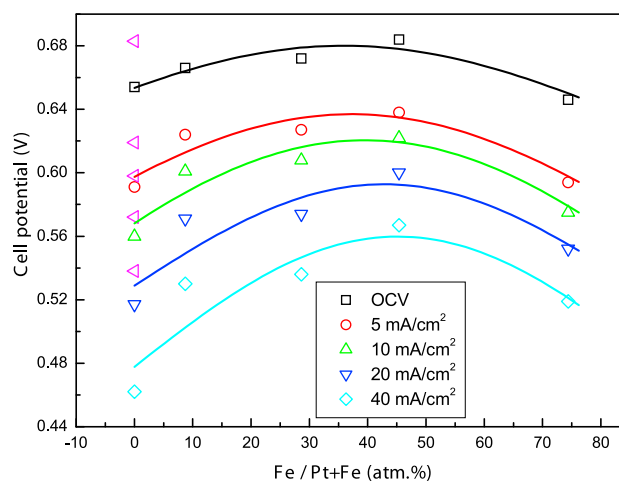

Fig. 8 – DMFC output potential *vs.* Fe atomic percentage in Pt–Fe/C catalyst at operation current density of 5, 10, 20 and 40 mA/cm^2.

For ORR activity enhancement on the Pt–M/C catalysts, extensive investigations [18–43] were conducted and several hypothesized mechanisms were provided [10,19,22–29,33]. Jalan and Taylor studied the ORR at Pt alloys supported on carbon black for PAFCs and claimed that the shortening of Pt–Pt interatomic distances by alloying leads to the enhancement of Pt catalytic activity for ORR [19]. It was shown that the lattice contractions due to alloying resulted in a favorable Pt–Pt distance for the dissociative adsorption of O_2, while maintaining the favorable electronic property of Pt [19,33]. Mukerjee and Srinivasan found no electronic structure change on basis of the results with XRD and XPS at supported Pt binary alloys in PEFCs [23]. The same research group ratio-nalized the enhanced electrocatalysis later with in situ XANES and EXAFS on the basis of the interplay between the electronic (Pt d-vacancy) and geometric factors (Pt coordination number), and their effect on the chemisorption behavior of OH species from the electrolyte [24]. Extensive research on Pt single crystals strongly supports the mechanism of inhibition by anion adsorption (OH_{ads}) [27–29]. Watanabe's group prepared Pt alloys with Ni, Co, Fe by sputtering and investi-gated their ORR activity in perchloric acid solution. It was found that the optimum Pt–Fe ratio is 1:1. They claimed the improving activity of ORR is based on the increased d-electron vacancy of the skin Pt surface layer caused by underlying transition metal, such as Fe, Co, Ni. They also used STM and EQCM experiments to verify this mechanism [25,26]. Other hypotheses, Surface roughness [22] and H_2O_2 decomposition [40] mechanisms were also proposed to explain the enhanced ORR activity on Pt–M alloy catalysts.

Some researches on Pt–M/C alloy cathode catalysts for DMFCs have been reported [39–43]. Maillard et al. studied the effect of particle size of Pt/C on the methanol-tolerant oxygen reduction reaction by using RDE technique in 1.0 M H_2SO_4 + 0.5 M CH_3OH. It was found that the mass activity of Pt increased continuously with a decrease in Pt particle size from 4.6 to 2.3 nm. While in methanol free electrolyte the mass activity was roughly independent of particle size, when $d < 3.5$ nm [39]. Shukla et al. used impregnation method prepared Pt–Fe/C (1:1 in atomic ratio) catalyst and found the Pt–Fe/C has methanol-tolerant ORR activity, which is attributed to its fct alloy structure and higher proportion of Pt active sites [41]. Very recently, Malheiro et al. investigated Pt–Fe/C cata-lysts with Pt:Fe composition of 50:50 and 70:30, and found that a Pt-rich surface has an enhanced ORR performance, but an inferior methanol tolerance ability in methanol containing solutions [43]. Our study suggested that Pt–Fe/C as cathode catalyst in DMFC does not show size sensitive effect: the catalysts with smaller Pt particle size and higher surface show higher ORR activity in DMFC. In addition, the alloy degree of Pt–Fe nanoparticles plays another important role in determining the ORR activity and overall DMFC performance. Better Pt–Fe alloy structures improved ORR activity in DMFC tests. However, Pt–Fe/C-d has not shown further improvement in ORR activity, although it has the smallest particle size and lattice parameter. This is probably because more non-alloyed Fe aggregates covering catalyst surface, thus deteriorating the ORR activity [21]. Pt–Fe/C-d may have less Pt-rich surface due to high Fe content, which will lead to lower methanol-tolerant ability, as suggested by Ref. [43]. Therefore, the sample-

d cannot further improve the DMFC performance. Under identical operation conditions of 90 °C cell temperature and 0.2 MPa oxygen back pressure, the power density of the DMFC with Pt–Fe/C-c cathode catalyst can reach 120 mW cm^{-2}, while that of the DMFC with Pt/C cathode catalyst is only 92 mW cm^{-2}. The stability and life-time of the Pt–Fe/C catalyst are required to be tested in the future work.

4. Conclusion

In this paper, we prepared a series of nanostructured Pt–Fe/C with varying Pt:Fe ratio by a modified EG method and subse-quent heat-treatment at 900 °C under H_2/Ar (10 vol%) atmo-sphere. XRD analysis show that Pt–Fe/C catalysts have small crystalline particle size and form better Pt–Fe alloy with Fe amount increasing. TEM images evidence that small Pt–Fe nanoparticles homogeneously deposited on carbon support and addition of Fe can effectively prevent Pt particles agglomeration. EDX and ICP-AES show that Fe precursor cannot be fully reduced and deposited on carbon support through the adopted EG reduction approach. CV curves show that the ECSA of Pt–Fe/C catalyst increases with Fe atomic percentage increasing from 0 to ca. 50%, and then decreases with more Fe in the Pt–Fe/C catalyst. RDE tests show that the Pt–Fe/C with a Pt:Fe ratio of 1.2:1 has the highest mass activity and specific activity to oxygen reduction reaction (ORR). The optimized lattice parameter of Pt–Fe alloy is around 3.894 Å for ORR. DMFC tests show that the Pt–Fe/C with Pt:Fe ratio of 1.2:1 has the highest fuel cell performance among all Pt/C and other Pt–Fe/C catalysts at testing condition of 90 °C cell temperature and 0.2 MPa oxygen back pressure, which could be attributed to its smaller particle size (3.2 nm) and better Pt–Fe alloy structure (lattice parameter of 3.894 Å).

REFERENCES

[1] Basic research needs for the hydrogen economy. U.S. Department of Energy, Office of Basic Science; 2004.
[2] Vielstich W, Lamn A, Gasteiger H. Handbook of fuel cells. John Wiley & Sons Inc.; 2004.
[3] Hamnett A. Mechanism and electrocatalysis in the direct methanol fuel cell. Catal Today 1997;38:445.
[4] McNicol BD, Rand DAJ, Williams KR. Direct methanol-air fuel cells for road transportation. J Power Sources 1999;83:15.
[5] Wasmus S, Kuver A. Methanol oxidation and direct methanol fuel cells: a selective review. J Electroanal Chem 1999;461:14.

[6] Ren X, Zelenay P, Thomas S, Davey J, Gottesfeld S. Recent advances in direct methanol fuel cells at Los Alamos National Laboratory. J Power Sources 2000;86:111.

[7] Arico AS, Srinivasan S, Antonucci V. DMFCs: from fundamental aspects to technology development. Fuel Cells 2001;2:133.

[8] Li W, Liang C, Zhou W, Qiu J, Zhou Z, Sun G, et al. Preparation and characterization of multi-walled carbon nanotube-supported platinum for cathode catalyst of direct methanol fuel cells. J Phys Chem B 2003;107:6292.

[9] Kinoshita K. Electrochemical oxygen technology. New York: John Wiley & Sons Inc.; 1992.

[10] Gasteiger HA, Kocha SS, Sompalli B, Wagner FT. Activity benchmarks and requirements for Pt, Pt-alloy, and non-Pt oxygen reduction catalysts for PEMFCs. Appl Catal B Environ 2005;56:9.

[11] Trapp V, Christensen P, Hamnett A. New catalysts for oxygen reduction based on transition-metal sulfides. J Chem Soc Faraday Trans 1996;92:4311.

[12] Reeve R, Christensen P, Hamnett A, Haydock S, Roy S. Methanol tolerant oxygen reduction catalysts based on transition metal sulfides. J Electrochem Soc 1998;145:3463.

[13] Gojkovic SL, Gupta S, Savinell RF. Heat-treated iron(III) tetramethoxyphenyl porphyrin chloride supported on high-area carbon as an electrocatalyst for oxygen reduction – part II. Kinetics of oxygen reduction. J Electroanal Chem 1999;462:63.

[14] Schmidt TJ, Paulus UA, Gasteiger HA, Alonso-Vante N, Behm RJ. Oxygen reduction on Ru1.92Mo0.08SeO4, Ru/carbon, and Pt/carbon in pure and methanol-containing electrolytes. J Electrochem Soc 2000;147:2620.

[15] Tributsch H, Bron M, Hilgendorff M, Schulenburg H, Dorbandt I, Eyert E, et al. Methanol-resistant cathodic oxygen reduction catalysts for methanol fuel cells. J Appl Electrochem 2001;31:739.

[16] Ralph TR, Hogarth MP. Catalysis for low temperature fuel cells: Part 1: the cathode challenges. Platinum Met Rev 2002;46:3.

[17] Antolini E. Formation of carbon-supported PtM alloys for low temperature fuel cells: a review. Mater Chem Phys 2003;78:563.

[18] Jalan V. Activity enhancement of platinum by alloying with base metals. J Electrochem Soc 1982;129:C115.

[19] Jalan V, Taylor EJ. Importance of interatomic spacing in catalytic reduction of oxygen in phosphoric-acid. J Electrochem Soc 1983;130:2299.

[20] Kim KT, Kim YJ, Chung JS. Effect of surface roughening on the catalytic activity of electrocatalysts for the oxygen reduction in phosphoric-acid fuel cell. J Electrochem Soc 1995;142:1531.

[21] Kim KT, Hwang JT, Kim YG, Chung JS. Surface and catalytic properties of iron–platinum carbon electrocatalysts for cathodic oxygen reduction in PAFC. J Electrochem Soc 1993; 140:31.

[22] Paffett MT, Beery JG, Gottefeld S. Oxygen reduction at Pt0.65CR0.35, Pt0.2CR0.8 and roughened platinum. J Electrochem Soc 1988;135:1431.

[23] Mukerjee S, Srinivasan S. Enhanced electrocatalysis of oxygen reduction on platinum alloys in proton-exchange membrane fuel cells. J Electrochem Soc 1993;357:201.

[24] Mukerjee S, Srinivasan S, Soriaga M, Mcbrieen J. Role of structural and electronic-properties of Pt and Pt alloys on electrocatalysis of oxygen reduction – an in-situ XANES and EXAFS investigation. J Phys Chem B 1995;99:4577.

[25] Toda T, Igarashi H, Uchida H, Watanabe M. Enhanced of the electroreduction of oxygen on Pt alloys with Fe, Ni, and Co. J Electrochem Soc 1999;146:3750.

[26] Toda T, Igarashi H, Watanabe M. Enhancement of electrocatalytic O_2 reduction on Pt–Fe alloys. J Electroanal Chem 1999;460:258.

[27] Climent V, Markovic NM, Ross PN. Kinetics of oxygen reduction on an epitaxial film of palladium on Pt(111). J Phys Chem B 2000;104:3116.

[28] Stamenkovic V, Schmidt TJ, Ross PN, Markovic NM. Surface composition effects in electrocatalysis: kinetics of oxygen reduction on well defined Pt3Ni and Pt3Co alloy surfaces. J Phys Chem B 2002;106:11970.

[29] Stamenkovic V, Fowler B, Mun BS, Wang GF, Ross PN, Lucas CA, et al. Improved oxygen reduction activity on Pt3Ni(111) via increased surface site availability. Science 2007;315:493.

[30] Brankovic SR, Wang X, Adzic RR. Metal monolayer deposition by replacement of metal adlayers on electrode surfaces. Surf Sci 2001;474:173.

[31] Zhang JL, Vukmirovic MB, Xu Y, Mavrikakis M, Adzic RR. Controlling catalytic activity of platinum-monolayer electrocatalysts for oxygen reduction with different substrates. Angew Chem Int Ed 2005;4:2132.

[32] Zhang JL, Sasaki K, Sutter E, Adzic RR. Stabilization of platinum oxygen-reduction electrocatalysts using gold clusters. Science 2007;315:220.

[33] Koh S, Strasser P. Electrocatalysis on bimetallic surfaces: modifying catalytic reactivity for oxygen reduction by voltammetric surface dealloying. J Am Chem Soc 2007;129: 12624.

[34] Min MK, Cho JK, Cho KW, Kim H. Particle size and alloying effects of Pt-based alloy catalysts for fuel cell applications. Electrochim Acta 2000;45:4211.

[35] Neergat M, Shukla A, Gandhi K. Platinum-based alloys as oxygen-reduction catalysts for solid-polymer-electrolyte direct methanol fuel cells. J Appl Electrochem 2001;31:373.

[36] Shukla AK, Neergat M, Bera P, Jayaram V, Hegde M. An XPS study on binary and ternary alloys of transition metals with platinized carbon and its bearing upon oxygen electroreduction in direct methanol fuel cells. J Electroanal Chem 2001;504:111.

[37] Xiong L, Kannan A, Manthiram A. Pt–M (M = Fe, Co, Ni and Cu) electrocatalysts synthesized by an aqueous route for proton exchange membrane fuel cells. Electrochem Commun 2002;4:898.

[38] Hiroshima K, Asaoka T, Noritake T, Ohya Y, Morimoto Y. PEFC cathode alloy catalysts prepared by a novel process using a chelating agent. Fuel Cells 2002;2:1.

[39] Maillard F, Martin M, Gloaguen F, Leger J. Oxygen electroreduction on carbon-supported platinum catalysts. Particle-size effect on the tolerance to methanol competition. Electrochim Acta 2002;47:3431.

[40] Li W, Zhou W, Zhou Z, Li H, Zhou Z, Zhou B, et al. Nanostructured Pt–Fe/C as cathode catalyst in direct methanol fuel cell. Electrochim Acta 2004;49:1045.

[41] Shukla AK, Raman R, Choudhury N, Priolkar K, Sarode P, Emura S, et al. Carbon-supported Pt–Fe alloy as a methanol-resistant oxygen-reduction catalyst for direct methanol fuel cells. J Electroanal Chem 2004;563:181.

[42] Yang H, Coutanceau C, Leger JM, Alonso-Vante N, Larmy C. Methanol tolerant oxygen reduction on carbon-supported Pt–Ni alloy nanoparticles. J Electroanal Chem 2005;205:305.

[43] Malheiro AR, Perez J, Villullas HM. Surface structure and electronic properties of Pt−Fe/C nanocatalysts and their relation with catalytic activity for oxygen reduction. J Power Sources; 2009;. doi:10.1016/j.jpowsour.2009.11.096.

[44] Sun SH, Murray GB, Weller D, Folks L, Moser A. Monodisperse FePt nanoparticles and ferromagnetic FePt nanocrystal superlattices. Science 2000;287:1989.

[45] Sun SH, Anders S, Thomson T, Baglin JEE, Toney MF, Hamann HF, et al. Controlled synthesis and assembly of FePt nanoparticles. J Phys Chem B 2003;107:5419.

[46] Luo J, Njoki PN, Lin Y, Wang LY, Zhong CJ. Activity-composition correlation of AuPt alloy nanoparticle catalysts in electrocatalytic reduction of oxygen. Electrochem Commun 2006;8:581.

[47] Luo J, Wang LY, Mott D, Njoki PN, Kariuki N, Zhong CJ, et al. Ternary alloy nanoparticles with controllable sizes and composition and electrocatalytic activity. J Mater Chem 2006; 16:1665.

[48] Liu ZF, Shamsuzzoha M, Ada ET, Reichert WM, Nikles DE. Synthesis and activation of Pt nanoparticles with controlled size for fuel cell electrocatalysts. J Power Sources 2007; 164:472.

[49] Yano H, Kataoka M, Yamashita H, Uchida H, Watanabe M. Oxygen reduction activity of carbon-supported Pt–M (M = V, Ni, Cr, Co, and Fe) alloys prepared by nanocapsule method. Langmuir 2007;23:6438.

[50] Li W, Haldar P. Supportless PdFe nanorods as highly active electrocatalyst for proton exchange membrane fuel cell. Electrochem Commun 2009;11:1195.

[51] Li W, Chen Z, Xu L, Yan Y. A solution-phase synthesis method to highly active PtCo/C catalysts for proton exchange membrane fuel cell. J Power Sources 2010;195:2534–40.

[52] Toshima N, Yonezawa T. Bimetallic nanoparticles - novel materials for chemical and physical applications. New J Chem 1998;22:1179.

[53] Wang Y, Ren JW, Deng K, Gui LL, Tang YQ. Preparation of tractable platinum, rhodium, and ruthenium nanoclusters with small particle size in organic media. Chem Mater 2000; 12:1622.

[54] Li W, Liang C, Qiu J, Zhou W, Han H, Wei Z, et al. Carbon nanotubes as support for cathode catalyst of a direct methanol fuel cell. Carbon 2002;40:791.

[55] Liu ZL, Lin XH, Lee JY, Zhang W, Han M, Gan L. Preparation and characterization of platinum-based electrocatalysts on multiwalled carbon nanotubes for proton exchange membrane fuel cells. Langmuir 2002;18:4054.

[56] Zhou Z, Wang S, Zhou W, Wang G, Jiang L, Li W, et al. Novel synthesis of highly active Pt/C cathode electrocatalyst for direct methanol fuel cell. Chem Commun 2003;3:394.

[57] Zhou W, Zhou Z, Song S, Li W, Sun G, Tsiakaras P, et al. Pt based anode catalysts for direct ethanol fuel cells. Appl Catal B Environ 2003;46:273.

[58] Li H, Xin Q, Li W, Zhou Z, Jiang L, Yang S, et al. An improved palladium-based DMFC cathode catalyst. Chem Commun 2003;23:2776.

[59] Zhou W, Li W, Song S, Zhou Z, Jiang L, Sun G, et al. Bi- and tri-metallic Pt-based anode catalysts for direct ethanol fuel cell. J Power Sources 2004;131:217.

[60] Jiang L, Zhou Z, Li W, Zhou W, Song S, Li H, et al. Effect of treatment in different atmosphere on Pt3Sn/C electrocatalysts for ethanol electro-oxidation. Energy Fuels 2004;18:866.

[61] Zhao X, Li W, Jiang L, Zhou W, Xin Q, Yi B, et al. Mutil-wall carbon nanotubes supported PtSn nanoparticles as anode catalyst for direct ethanol fuel cells. Carbon 2004;42:3263.

[62] Li W, Wang X, Chen Z, Waje M, Yan Y. Carbon nanotube film by filtration as cathode catalyst support for proton exchange membrane fuel cell. Langmuir 2005;21:9386.

[63] Li W, Wang X, Chen Z, Waje M, Yan Y. Pt–Ru supported on double walled carbon nanotubes as high performance anode catalysts for direct methanol fuel cells. J Phys Chem B 2006;110:15353.

[64] Knupp LS, Li W, Paschos O, Murray TM, Snyder J, Haldar P. The effect of experimental parameters on the synthesis of CNT and CNF supported Pt by polyol processing techniques. Carbon 2008;46:1276.

[65] Li W, Waje M, Chen Z, Larsen P, Yan Y. Platinum nanoparticles supported on stacked-cup carbon nanofibers as electrocatalysts for proton exchange membrane fuel cell. Carbon; 2009;. doi:10.1016/j.carbon.2009.11.017.